IEEE Access
Multidisciplinary ⋮ Rapid Review ⋮ Open Access Journal

Received June 3, 2021, accepted June 30, 2021, date of publication July 5, 2021, date of current version July 13, 2021.

Digital Object Identifier 10.1109/ACCESS.2021.3094579

Synchronous Online Monitoring of Rotational Speed and Temperature for Rotating Parts in High Temperature Environment

CHEN LI[1,2], MANGU JIA[1,2], YANAN XUE[1], YINGPING HONG[1], QIYUN FENG[1], PENGYU JIA[1], HAOYUE LU[1], AND JIJUN XIONG[1,2]

[1]Science and Technology on Electronic Test and Measurement Laboratory, North University of China, Taiyuan 030051, China
[2]Key Laboratory of Instrumentation Science and Dynamic Measurement, Ministry of Education, North University of China, Taiyuan 030051, China

Corresponding author: Jijun Xiong (xiongjijun@nuc.edu.cn)

This work was supported in part by the China Postdoctoral Science Foundation under Grant 2019M661071, and in part by the China Aviation Development Group Industry-University-Research Cooperation Project under Grant HFZL2020CXY019.

ABSTRACT Rotational speed and temperature measurements of an engine blade surface play a vital role in the performance detection of an engine. We proposed a wireless passive LC sensor based on thick-film integration technology to integrate the sensor in situ on the surface of the rotating part, which can be used to monitor the rotational speed and temperature of the rotating part. The reflection signal generated by the impedance mismatch is output in the form of voltage through the detection circuit such that the synchronous online measurement of rotational speed and temperature is realized by analyzing the time slot of adjacent troughs and the amplitude of the output voltage. In addition, we used laser drilling, screen printing, high-temperature sintering, and other technologies to integrate the sensor in situ on the surface of the ceramic turntable, which is lightweight. Finally, the test was conducted by setting up a rotational speed-high-temperature composite experimental platform, and the results showed that the sensor can work normally in the range of 25–830°C, and the rotational speed measurement range was 50–400rpm. The consistency of the rotational speed measurement was suitable, the maximum error was less than 1%, and the work was stable within 180 min.

INDEX TERMS High temperature, high temperature rotating environment, *in situ* integration, rotational speed, wireless measurement.

I. INTRODUCTION

As one of the key components of airplanes and automotives, engines contain numerous rotating parts, including blades, bearing brackets, and shafts, which work in harsh environments, such as high rotational speeds and high temperatures [1]–[5]. Therefore, monitoring rotational speed and temperature parameters is vital for the safe and reliable operation of an engine. For instance, engine blades are extremely vulnerable to thermal corrosion by high-temperature airflow during aircraft operation; therefore, real-time online monitoring of the rotational speed and temperature parameters of the blades will improve the reliability of the engine and reduce the damage rate of the blades [6]–[8].

The associate editor coordinating the review of this manuscript and approving it for publication was M. Saif Islam.

In general, a rotational speed sensor based on the contact measurement principle is installed on the surface of the rotating component directly such that the signal transmission electrical lead runs with the rotating component, causing problems, such as inaccurate test results and damage to the test device. Thus, numerous non-contact rotational speed sensors have been investigated to measure the rotational speed. In 2012, Li *et al.* [9] from Wuhan University developed a rotational speed sensor using the fiber Bragg grating as a sensitive component, which measured the rotational speed by converting the speed into grating strain. However, this type of optical sensor has strict requirements for the optical path transmission of a dust and barrier-free environment. In addition, the demodulation circuit of an optical fiber sensor is complex. Therefore, it has certain limitations in its application. Magnetic sensors have also been developed for rotational speed measurement, including magnetoresistive,

magneto-electric, eddy current, and electrostatic. In 2001, Giebeler *et al.* [10] presented a giant magnetoresistance sensor with a full wheatstone bridge for rotational speed sensing. In 2016, Wu *et al.* [11] demonstrated a rotational speed sensor based on the magneto-electric effect; the rotational speed sensor could measure the rotational speed within 1000rpm, and the measurement error was approximately 3%. Nevertheless, both of the aforementioned sensors are susceptible to the environment and have a narrow measurement bandwidth. In 2019, Mirzaei *et al.* [12] developed a rotational eddy current speed sensor and analyzed its performance through finite element simulations and experiments. However, the unevenness on the surface of the measured object, such as nicks and grooves, affects the measurement results and causes measurement errors. The electrostatic sensor designed by Wang *et al.* [4], [13], [14] transfers the charge generated by the friction between the rotating object and air to the sensor through electrostatic induction and then realizes the rotational speed measurement by subsequent algorithm processing. However, the lower the rotational speed, the less charge generated by the turntable, and, thus, this technique is not suitable for measuring low rotational speeds. In recent years, other methods have also been developed to test rotational speeds [15]–[18]. However, different measurement approaches have limitations. The noise signal generated by the engine operation is superimposed on the vibration signal, which will cause serious interference to the extraction and analysis of the vibration signal, resulting in a low accuracy of the measurement of the rotational speed based on the instantaneous speed evaluation technology of the vibration signal. None of the above-mentioned sensors involve rotational speed measurement in a high-temperature environment, and most of the internal moving parts of the engine work in a high-temperature environment. Therefore, it is particularly important to measure the temperature of the engine parts. In general, to avoid lead corrosion and combustion damage in a high-temperature environment, it is important to choose sensors that do not require leads for measurement. Simultaneously, compared with offline monitoring, online monitoring can always reflect the changing state of the blade temperature and other parameters [19]. For example, online measurement of engine blade temperature in a high-temperature environment uses thermal imaging phosphor, optical pyrometer [20]–[22], etc. and the temperature measurement of 700°C on the turbine blade surface was realized through thermal imaging phosphorescent coating. However, thermal imaging phosphors require optical components, which hinder the use of sensors for condition monitoring applications owing to space and airflow constraints. The radiation reflected from the high-temperature environment causes serious errors in the measurement of the optical pyrometer. Therefore, when an optical sensor is used to measure the temperature, the reflection error and dust in the air will affect the measurement to some extent. Passive RF LC transmission technology based on the principle of non-contact measurement has the advantages of high working temperature and convenient reading; it is widely used for parameter measurements in high-temperature environments, such as temperature and pressure measurements, which have a wide range of applications [23]–[26]. To date, wireless passive LC dual-parameter sensors mostly use dual LC-sensitive circuits, and the crosstalk between the inductance coils causes inaccurate measurement results.

Therefore, in this study, we proposed a wireless passive sensor to monitor rotational speed and temperature synchronously, allowing in situ integration of post-membrane technology as the fabrication process and electromagnetic induction principle as the transmission method to extract characteristic signals wirelessly. The sensor only contained a single LC circuit with Ag paste as the material. The experimental performance shows that the sensor can work normally at rotational speeds ranging from 50–400rpm and temperatures ranging from 25–830°C. The sensor prepared in this study is lightweight, along with the wireless signal extraction method, which makes it promising for in situ synchronization online monitoring of rotational speed and temperature in harsh environments, such as turbine blades and bearing cages of aero-engines.

II. MEASUREMENT PRINCIPLE

Based on the electromagnetic coupling principle, the equivalent model of the measurement principle of the designed sensor and antenna is shown in Figure 1, in which the sensor and antenna are located in a high-temperature and high-rotation environment, and the measurement circuit are located in a room-temperature environment. The RF signal source provides the sine signal with fixed frequency for the antenna, and the reflection signal caused by the impedance mismatch between the sensor and the antenna is input into the measuring circuit through the coupler, it is displayed and saved in the oscilloscope in the form of a semi-sinusoidal voltage after envelope detection by measuring circuit.

According to the resonance principle, when the resonance frequency of the sensor is the same as that of the signal source, the energy and signal are exchanged between the sensor and the antenna. Therefore, the signal source frequency in the measurement circuit is the resonance frequency of the sensor. When the sensor runs with the rotating parts in a high-temperature environment, the horizontal distance between the sensor and the antenna changes periodically (specifically, from large to small and then increases), leading to a change in the electromagnetic coupling strength between the sensor and the antenna, which is reflected in the change in the mutual inductance coefficient M_{sa} between the sensor and the antenna. This can be expressed as [27], (1) as shown at the bottom of the next page, where μ_0 is the vacuum permeability and R is the distance between two the points between the inductance of the sensor and the antenna. Further, a and b are the radii of the two coils, h is the vertical distance between the centers of the two coils, x is the horizontal offset distance of the centers, and φ_1 and φ_2 are the angles between the two coils and the horizontal line. In an ideal case, the impedance of the antenna, sensor, measurement circuit, and transmission

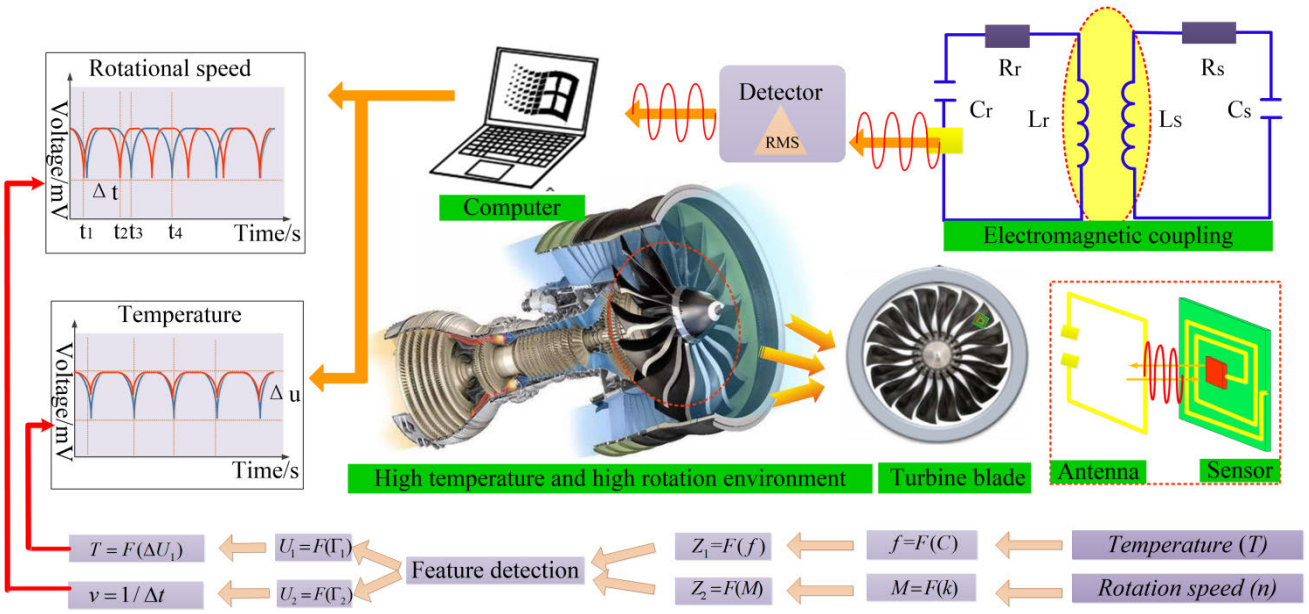

FIGURE 1. Schematic diagram of the sensor test principle and structure.

line are completely matched, and the RF input signal is not reflected, making the reflection coefficient infinitely small. However, practically, the entire measurement system cannot achieve a complete impedance match. Consequently, when the mutual inductance M_{ab} changes with the horizontal distance between the sensor and antenna, the reflection coefficient Γ at the antenna also changes. Because the characteristic impedance of the transmission line and the measurement circuit is 50 Ω in this study, the expression of the reflection coefficient Γ is [28], (2) as shown at the bottom of the page, where C_s is the equivalent capacitance of the sensor, R_a is the parasitic resistance at the circuit of the sensor, and ω is the angular frequency. The reflection coefficient Γ passes through the coupler and the detection circuit and is finally converted into a semi-sinusoidal voltage U_{out} for the output. The specific expression is as follows:

$$U_{out} = G_{env} \cdot C_{31} \cdot \Gamma = 1.46 C_{31} \cdot \Gamma \tag{3}$$

where G_{env} represents the amplification gain of the detection circuit with a value of 1.46 V and C_{31} represents the coupling coefficient between the coupling port of the third port and the input port of the coupler, respectively.

With the periodic rotation of the rotating parts, when the sensor and antenna are in the opposite position, implying that their inductance coils are coaxial, the coupling coefficient appears at the maximum value, the amplitude of the emission coefficient Γ is the minimum, and the output voltage appears at the minimum value. Therefore, the rotational speed measurement can be realized by analyzing the adjacent trough time slots of the output voltage with the specific expression as follows:

$$v = F(t) = \frac{1}{t_2 - t_1} \tag{4}$$

where t_1 and t_2 represent the time when the output voltage appears at the minimum in turn. In addition, as the temperature increases, the equivalent capacitance C_s of the sensor changes, leading to an offset in the resonant frequency of the sensor. As the magnetic field is weakened by the temperature increase, the energy received and reflected by the sensor is reduced; therefore, the coupling effect between the sensor and the antenna is weakened, which is reflected in the decrease in the output voltage. We can extract the output voltage trough to analyze the temperature effect because the sensor resistance with a small temperature change can be ignored; we mainly

$$\begin{cases} M_{sa} = F(R) = \dfrac{\mu_0}{4\pi} \oint_{l_1} \oint_{l_2} \dfrac{1}{R} d\vec{l}_1 d\vec{l}_2 \\ R = F(x) = \sqrt{a^2 + b^2 + h^2 + x^2 - 2ab\cos(\varphi_1 - \varphi_2) + 2xb\cos\varphi_2 - 2xa\cos\varphi_1} \end{cases} \tag{1}$$

$$\Gamma = F(M_{ab}) = 1 - \frac{100}{50 + R_a + j\omega L_r + \frac{\omega^2 M_{ab}^2}{R_s + j\omega L_s + \frac{1}{j\omega C_s}}} \tag{2}$$

focused on the capacitance change analysis [25], [29].

$$\varepsilon_r \propto T \tag{5}$$

$$C_s = F(\varepsilon_r) = \varepsilon_0 \frac{\varepsilon_r A}{d} \tag{6}$$

$$f_s = F(C_s) \frac{1}{2\pi\sqrt{L_s C_s}} \tag{7}$$

$$Z = R + j2\pi f L_r + \frac{(2\pi f)^2 M^2}{R_s + j(2\pi f L_s - \frac{1}{2\pi f C_s})} \tag{8}$$

$$\Gamma = F(Z) = \frac{Z - Z_0}{Z + Z_0}\bigg|_{Z_0=50\Omega} = 1 - \frac{100}{Z + 50} \tag{9}$$

$$T = F(U_{out}) \tag{10}$$

Here, A represents the area of the capacitor, d is the distance between the capacitor plates, ε_0 is the vacuum dielectric constant, and ε_r is the relative dielectric constant of alumina, which changes with temperature. R_s, R_r, L_s, L_r represent the resistance and inductance of the sensor and the antenna respectively, M represents the mutual inductance between the sensor and the antenna, Z represents the impedance of the antenna. The specific changes in the output voltage caused by the temperature and rotational speed are shown in Figure 1.

III. FABRICATION SENSOR

The designed sensor uses Ag (ESL9912) slurry as an electrode material and adopts thick-film integration technology to integrate in situ on the surface of the rotating parts. The technology can realize in situ integrated manufacturing of the rotational structure surface. The detailed fabrication steps are shown in Figure 2.

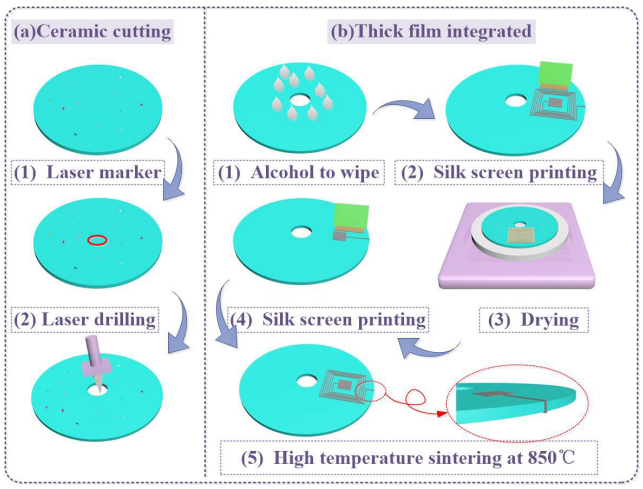

FIGURE 2. Fabrication process of the designed sensor.

First, we brick a hole with a diameter of 1 mm in the middle of the ceramic disc using laser drilling technology to connect with the rotating shaft.

Second, ethanol was used to clean the surface of the ceramic disc to ensure adhesion between the film and the ceramic substrate.

Subsequently, according to the optimized parameters, a spiral inductor template for screen printing was designed. By applying an appropriate amount of Ag electronic paste to the screen-printing plate, adjusting the distance between the screen plate and the ceramic plate, holding the scraper at an angle, and moving in a fixed direction at a certain rotational speed, part of the slurry is deposited on the surface of the ceramic plate by extrusion and bonding.

Thereafter, the ceramic substrate printed with the circuit pattern was put into the high and low temperature test box, the slurry was dried at 150°C for 10 min, and then the ceramic substrate was removed to allow it to cool naturally and flip over; Further, a spatula with a small amount of slurry was used to connect the inductance coil to the capacitor plate to form a closed LC circuit.

Finally, the ceramic plate with electrode pattern was sintered at 250°C for 20 min and then at 850°C for 40 min; after 40 min of heat preservation, the organic solvent in the slurry was removed and the metal electrode was tightly bonded with the ceramic substrate. The above steps realize the preparation of the surface LC loop of the rotating part.

The fabricated sensor is shown in Figure 3(a). An enlarged view of the sensor electrode under the microscope is shown

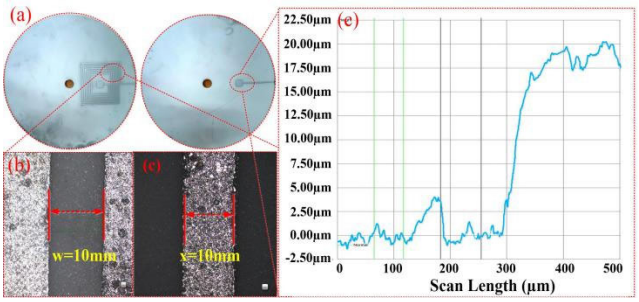

FIGURE 3. (a) Physical image of the sensor. (b) Inductance profile of the sensor under a confocal microscope. (c) Electrode thickness measured by the sensor under a step meter.

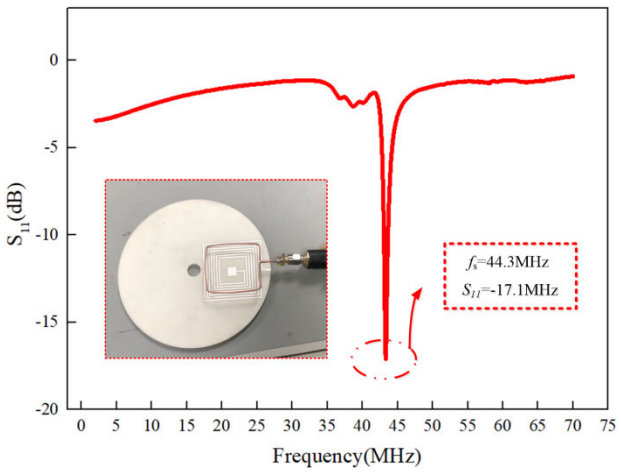

FIGURE 4. Coupling frequency of the sensor and antenna.

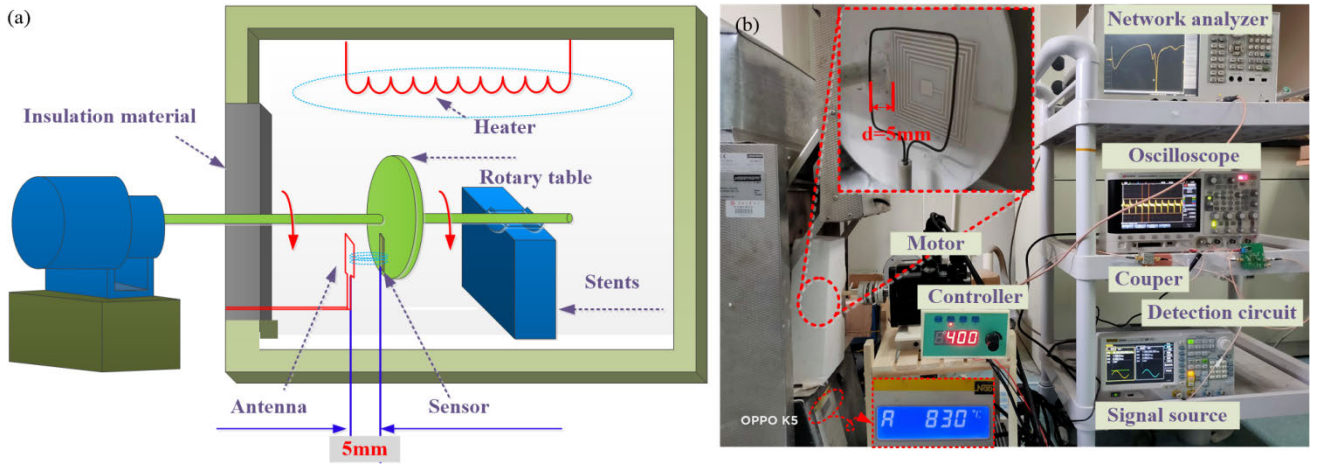

FIGURE 5. Scheme of the high-temperature and rotational speed composite environment testing system. (a) Principle of rotational speed and temperature. (b)Rotational speed and temperature measurement platform.

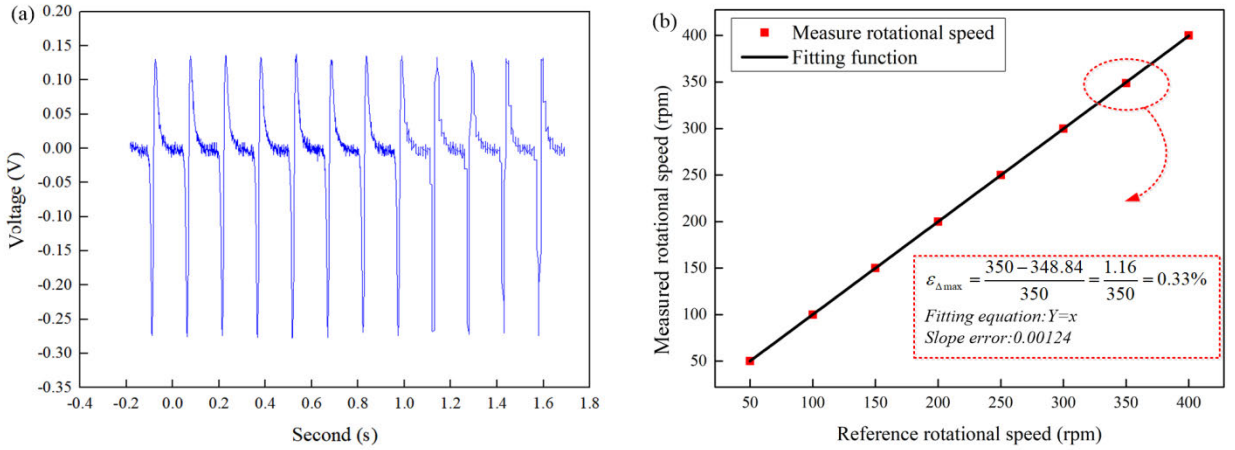

FIGURE 6. (a) Waveform diagram output by the oscilloscope at 400rpm. (b) Non-linear error ofthe measured rotational speed.

in Figures 3(b) and (c). As shown in the figure, the width of the sensor's inductance is 10 mm, and the width between adjacent inductances is 10 mm. As shown in Figure 3(d), the thickness of the sensor was found to be 20μm by observing the step meter. This indicates that the sensor can be thinly attached to the surface of the rotating parts, laying the foundation for subsequent use in blades and other parts. The return loss (S_{11}) is the reflected signal caused by the impedance mismatch, which reflects the signal transmission strength. The smaller the return loss, the better the performance of the designed sensor. We set the distance between the sensor and the antenna to 5 mm and then measured the coupling frequency between the antenna and the sensor using a network analyzer, as shown in Figure 4. It can be observed from the figure that the frequency between the antenna and the sensor is 44.3 MHz and S_{11} is -17.1 dB. The sensor structure designed in this study was reasonable.

IV. RESULT AND DISCUSSION

In this section, the platform construction, room-temperature rotational speed measurement, and high-temperature rotational speed measurement are explained.

A schematic of the high-temperature and rotational speed test platform is shown in Figure 5(a) and (b). The test platform is mainly divided into high-temperature and room-temperature zones. The high-temperature area mainly includes a muffle furnace, a high-temperature ceramic turntable, a rotating shaft, high-temperature supporting equipment, sensor and antenna, while the normal temperature area mainly includes the motor, detection circuit module, coupler, signal generation, and oscilloscope. The function of the detection circuit is mainly realized by the ADL5511 chip, the working temperature is -45-60°C, and it has excellent temperature stability. As shown in Figure 5(b), the muffle furnace was equipped with a heater, thermocouple, and temperature controller. Users can set the corresponding

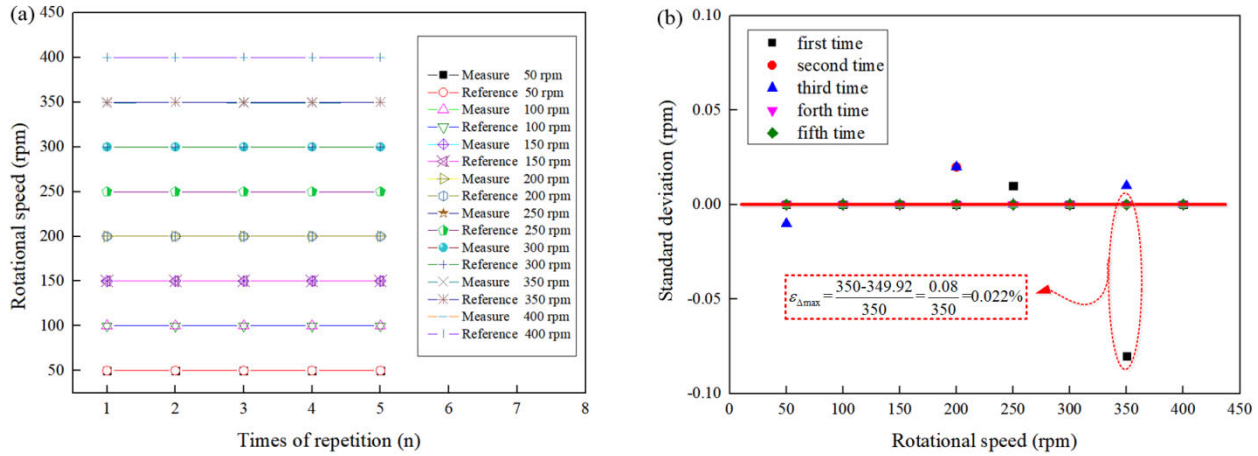

FIGURE 7. (a) Comparison between the measured and reference rotational speed. (b) Relative error of the multiple measured rotational speeds at room-temperature.

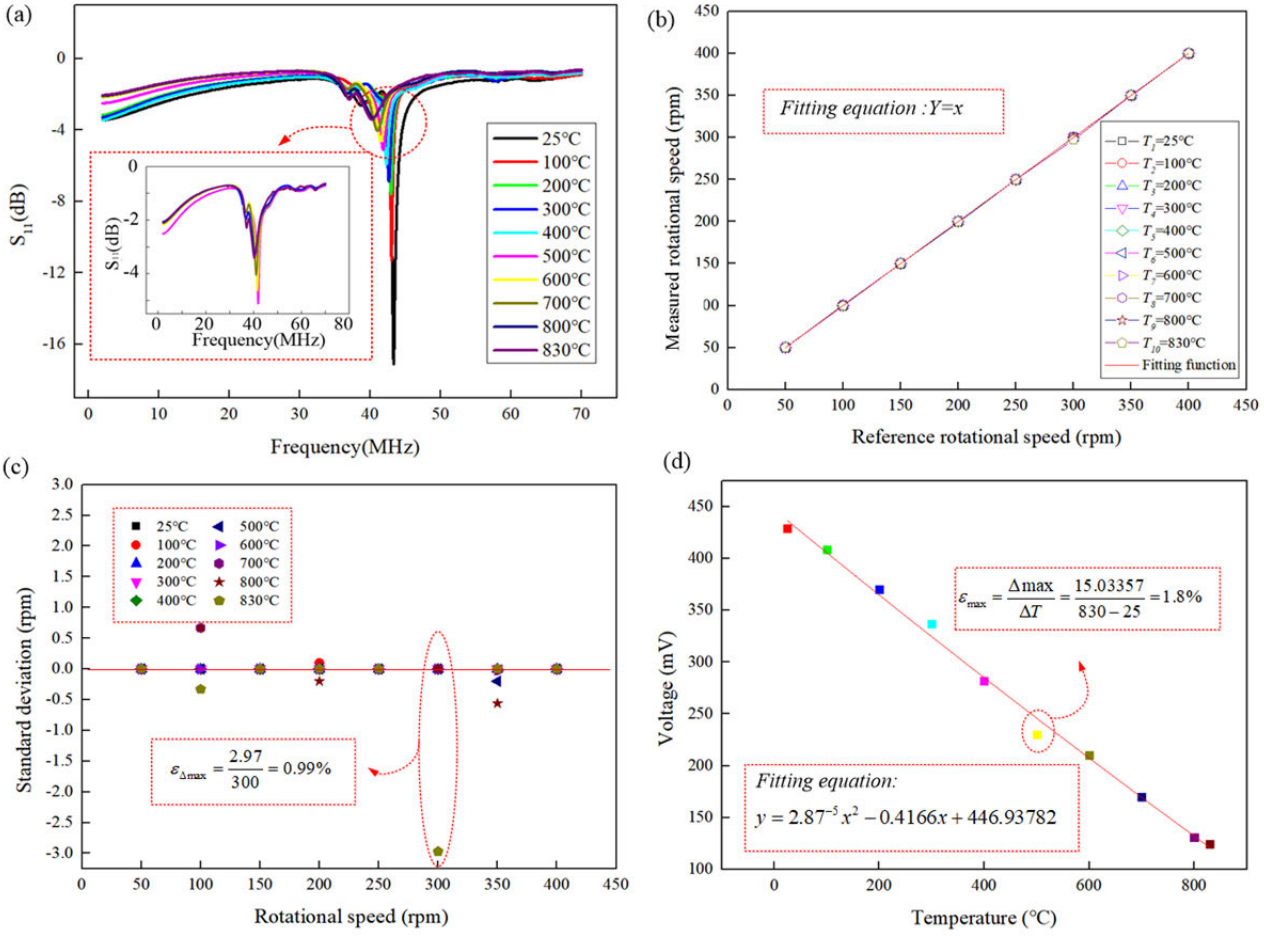

FIGURE 8. (a) Coupling frequency at different temperatures. (b) Rotational speed test at different temperatures. (c) Relative error of the measured rotational speed at different temperatures. (d) Voltage at the same rotational speed and different temperatures.

temperature curve through a digital display temperature program controller to automatically control the temperature. The high-temperature ceramic rotating shaft was placed in a muffle furnace, and the motor was connected to the high-temperature ceramic rotating disk through the rotating shaft to provide the rotational speed and high-temperature

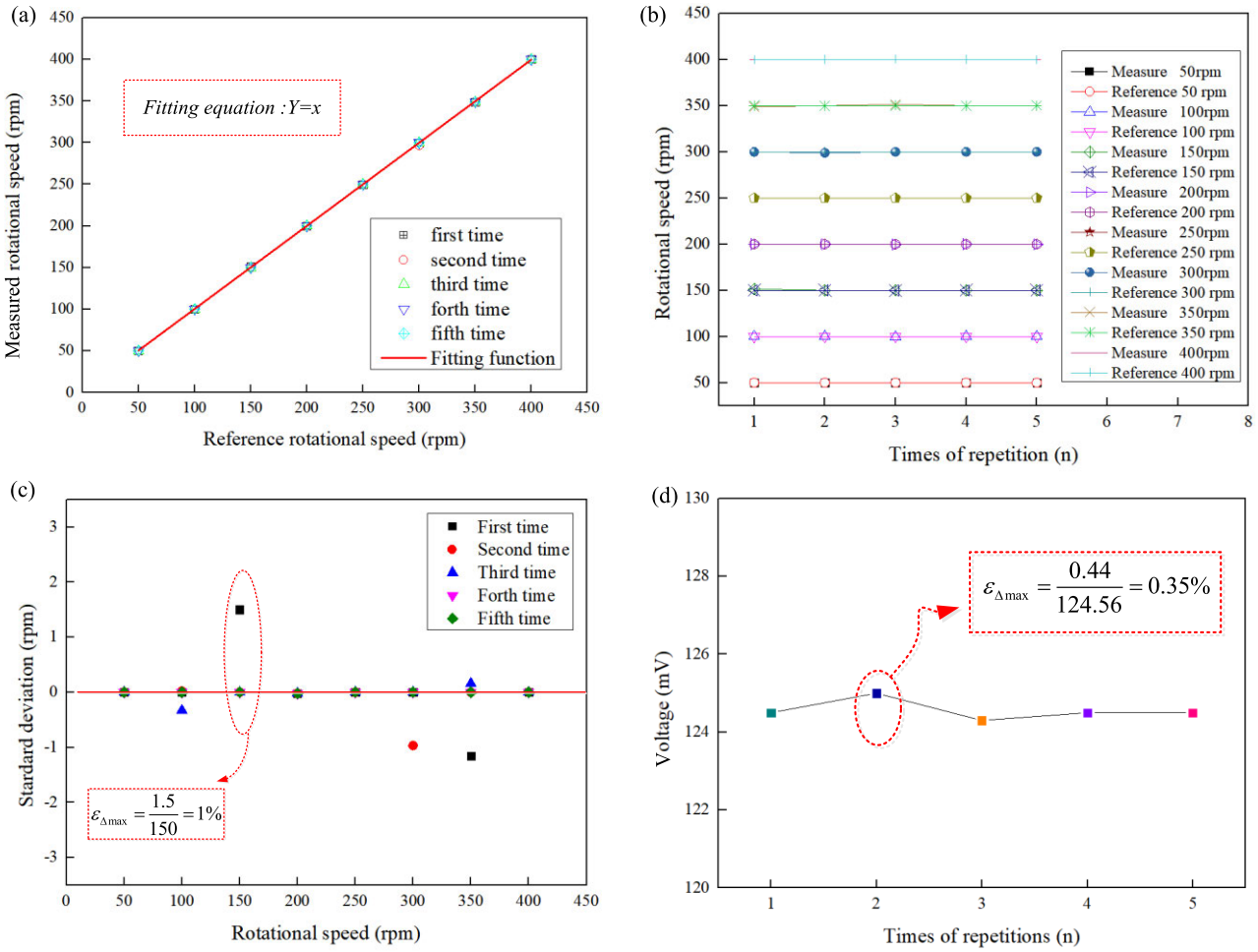

FIGURE 9. Performance of sensor at 830°C. (a) Result of five rotational speed tests of the sensor. (b) Comparison between the actual measured rotational speed and the given rotational speed of the motor. (c) Relative error of the multiple measured rotational speeds. (d) Sensor at 830 °C for multiple measurements of the oscilloscope output voltage.

environment for the sensor. The high-temperature and room-temperature zones are separated by mullite with a suitable heat insulation effect, and the antenna is installed at the interface of the muffle. The coupling distance between the sensor and antenna was set to 5 mm.

A. ROTATIONAL SPEED MEASUREMENT UNDER A ROOM-TEMPERATURE ENVIRONMENT

First, the performance of the sensor was measured at room temperature. The rotational speed of the motor was adjusted from 50 to 400rpm at 50rpm. The rotational speed of the motor was adjusted from 50 to 400rpm at 50rpm. The time point between the trough output by the oscilloscope was a cycle. Equation (4) was used to obtain the rotational speed measured by the sensor. The output waveform of the oscilloscope at 400rpm is shown in Figure 6 (a); Figure 6(b) shows the relationship between the measured rotational speed and the set rotational speed of the motor. From the figure, the actual rotational speed of the motor is almost the same as the measured rotational speed. At 350rpm, the maximum error was 0.022%.

To ensure the accuracy of the test results, the sensor was tested once every 30 min; after 5 times of testing, the results of motor rotational speed measurement as shown in Figure 7(a) were obtained. The measured rotational speed shown in the figure is the result of five measurements and the set value, as shown in Figure 7(b), which is the relative error between the measured rotational speed and the motor rotational speed. The above analysis shows that the maximum error is 0.022%, and the measured rotational speed and the motor rotational speed have a good consistency in a normal temperature environment.

B. ROTATIONAL SPEED MEASUREMENT UNDER A HIGH-TEMPERATURE ENVIRONMENT

To further explore the relationship between the rotational speed and the temperature measured by the sensor, the coupling frequencies between the sensor and the antenna are measured at 25, 100, 200, 300, 400, 500, 600, 700, 800, and

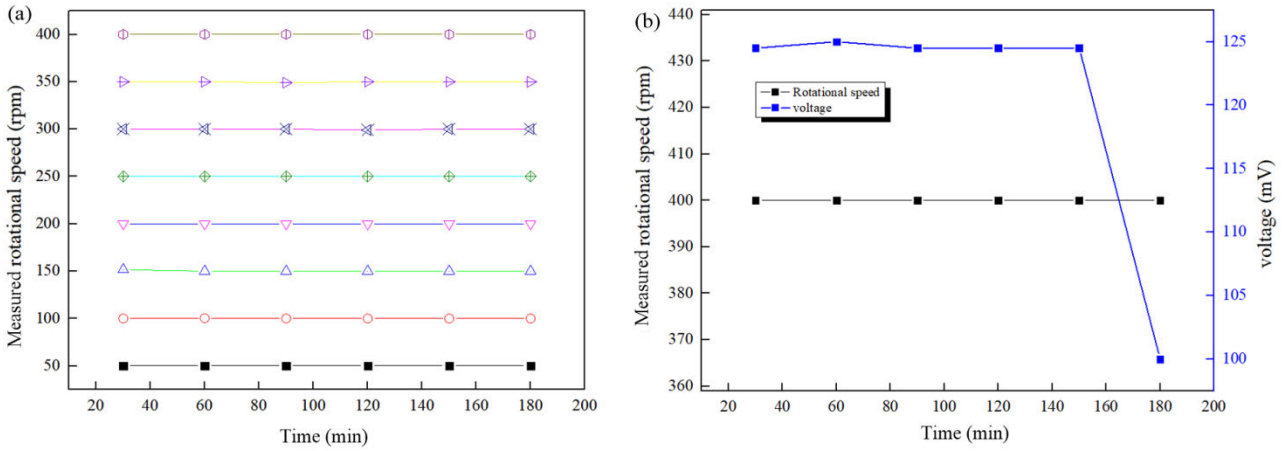

FIGURE 10. Stability measure at 830 °C. (a) Rotational speed of the sensor at 180 min. (b) Sensor at 830 °C for 180 min of the oscilloscope output voltage change.

830°C by the Network analyzer, and the results are shown in Figure 8(a). We can observe that the coupling frequency decreases from high to low temperature. This phenomenon is attributed to the dielectric constant of the substrate increasing with an increase in temperature, leading to an increase in the capacitance of the sensor; the coupling effect between the sensor and antenna is weakened and the coupling frequency is shifted. Subsequently, the output characteristics of the sensor are analyzed when the temperature and rotational speed change, and the influence of temperature on the rotational speed measurement is determined. The rotational speed of the sensor was tested at 25, 100, 200, 300, 400, 500, 600, 700, 800, and 830°C from 50 to 400rpm. Figure 8(b) shows the relationship between the measured rotational speed and the given rotational speed of the motor at different temperatures. Figure 8(c) shows the error between the measured rotational speed and the actual rotational speed at different temperatures. The maximum error was less than 0.99%. We found that the rotational speed can be measured at different temperatures, and the temperature has no effect on the rotational speed. Figure 8(d) shows the voltage amplitude of the oscilloscope at different temperatures at the same rotational speed. It can be observed from the figure that the voltage amplitude decreases with an increase in temperature at the same rotational speed, and the decreasing trend is nearly linear, as well as the maximum margin of error is no more than 1.8%.

The repeatability and stability tests of the sensor were performed at 830°C. The rotational speed of the sensor was measured every 30 min, as well as from 50 to 400rpm, as shown in Figure 9(a). The actual measured rotational speed was compared with the given rotational speed of the motor, as shown in Figure 9(b). The error analysis is shown in Figure 9(c). As can be observed from the diagram, at 830°C, the sensor can measure the rotational speed stably, the maximum error is 1.5 r/min, and the error is 1%. Figure 9(d) shows the output voltage amplitude of the sensor at the 830°C oscilloscope. We can observe that the sensor is also sensitive to temperature. The maximum error of the five repeatability tests is not more than 0.35%.

Next, we tested the stability of the sensor at 830°C, and the rotational speed and temperature of the sensor were measured every 30 min. As shown in Figures 10(a) and (b), the rotational speed of the sensor does not change much in 180min, but the voltage drops sharply in 180min during the temperature measurement; therefore, the sensor can operate for 180min, and if the sensor and the antenna are integrated into turbine blades and engine housings respectively, it is possible to realize the measurement of rotating parts in high-temperature, such as engine blades.

V. CONCLUSION

We demonstrated a wireless passive LC sensor based on thick-film integrated technology for the simultaneous online measurement of rotational speed and temperature in a high-temperature environment. The thick-film integration technology ensures the in-situ integration of the sensor on the surface of the component under test. The experimental tests were investigated in the built temperature-rotational speed composite platform. The results show that the sensor can measure the rotational speed and temperature simultaneously in the temperature range of 25–830°C, and the sensor can operate normally in the range of 50–400rpm, the maximum error is not more than 0.99%, and the change in temperature can be expressed by the output voltage of the oscilloscope. At 830°C, the relative error between the measured rotational speed and the reference rotational speed reaches a maximum of 1% and the stability of the sensor is 180min, which is important prospect for measuring the rotational speed and temperature of the rotating parts in extreme high-temperature environments in the future.

REFERENCES

[1] F. L. Duan, J. Li, J. Gao, G. Ding, and X. Cao, "Integrated fabrication of high-temperature microelectromechanical system sensor on aeroengine turbine blade," *J. Thermophys. Heat Transf.*, vol. 32, no. 3, pp. 826–829, 2018.

[2] B. Zaghari, A. S. Weddell, K. Esmaeili, I. Bashir, T. J. Harvey, N. M. White, P. Mirring, and L. Wang, "High-temperature self-powered sensing system for a smart bearing in an aircraft jet engine," *IEEE Trans. Instrum. Meas.*, vol. 69, no. 9, pp. 6165–6174, Sep. 2020.
[3] P. Mohankumar, J. Ajayan, R. Yasodharan, P. Devendran, and R. Sambasivam, "A review of micromachined sensors for automotive applications," *Measurement*, vol. 140, pp. 305–322, Jul. 2019.
[4] L. Wang, Y. Yan, Y. Hu, and X. Qian, "Rotational speed measurement through electrostatic sensing and correlation signal processing," *IEEE Trans. Instrum. Meas.*, vol. 63, no. 5, pp. 1190–1199, May 2014.
[5] N. Fernando, P. Arumugam, and C. Gerada, "Design of a stator for a high-speed turbo-generator with fixed permanent magnet rotor radius and volt–ampere constraints," *IEEE Trans. Energy Convers.*, vol. 33, no. 3, pp. 1311–1320, Sep. 2018.
[6] T. George, K.-A. Son, R. A. Powers, L. Y. D. Castillo, and R. Okojie, "Harsh environment microtechnologies for NASA and terrestrial applications," in *Proc. IEEE SENSORS*, Irvine, CA, USA, Oct. 2005, p. 6.
[7] Z. Habib, R. Parthasarathy, and S. Gollahalli, "Performance and emission characteristics of biofuel in a small-scale gas turbine engine," *Appl. Energy*, vol. 87, no. 5, pp. 1701–1709, May 2010.
[8] A. Saito, M. P. Castanier, and C. Pierre, "Effects of a cracked blade on mistuned turbine engine rotor vibration," *J. Vib. Acoust.*, vol. 131, no. 6, pp. 0610061–0610069, Dec. 2009.
[9] L. Wei, T. T. Hu, and Y. G. Tan, "Design and experimental test of fiber Bragg grating rotate speed sensor elastomer," *Appl. Mech. Mater.*, vols. 130–134, pp. 4073–4078, Oct. 2011.
[10] C. Giebeler, D. J. Adelerhof, A. E. T. Kuiper, J. B. A. van Zon, D. Oelgeschläger, and G. Schulz, "Robust GMR sensors for angle detection and rotation speed sensing," *Sens. Actuators A, Phys.*, vol. 91, nos. 1–2, pp. 16–20, Jun. 2001.
[11] Z. Shi, Q. Huang, G.-S. Wu, Y.-H. Xu, M. Yang, X.-J. Liu, C.-P. Wang, and J. Ma, "Design and development of a tachometer using magnetoelectric composite as magnetic field sensor," *IEEE Trans. Magn.*, vol. 54, no. 7, pp. 1–4, Jul. 2018.
[12] M. Mirzaei, P. Ripka, J. Vyhnanek, A. Chirtsov, and V. Grim, "Rotational eddy current speed sensor," *IEEE Trans. Magn.*, vol. 55, no. 9, pp. 1–10, Sep. 2019.
[13] L. Wang, Y. Yan, Y. Hu, and X. Qian, "Rotational speed measurement using single and dual electrostatic sensors," *IEEE Sensors J.*, vol. 15, no. 3, pp. 1784–1793, Mar. 2015.
[14] L. Wang, Y. Yan, and K. Reda, "Comparison of single and double electrostatic sensors for rotational speed measurement," *Sens. Actuators A, Phys.*, vol. 266, pp. 46–55, Oct. 2017.
[15] H. Lin and K. Ding, "A new method for measuring engine rotational speed based on the vibration and discrete spectrum correction technique," *Meas. J. Int. Meas. Confederation*, vol. 46, no. 7, pp. 2056–2064, 2013.
[16] X. Zhang, J. Chen, Z. Wang, N. Zhan, and R. Wang, "Digital image correlation using ring template and quadrilateral element for large rotation measurement," *Opt. Lasers Eng.*, vol. 50, no. 7, pp. 922–928, Jul. 2012.
[17] T. Wang, Y. Yan, L. Wang, and Y. Hu, "Rotational speed measurement through image similarity evaluation and spectral analysis," *IEEE Access*, vol. 6, pp. 46718–46730, 2018.
[18] T. Wang, Y. Yan, L. Wang, Y. Hu, and S. Zhang, "Instantaneous rotational speed measurement using image correlation and periodicity determination algorithms," *IEEE Trans. Instrum. Meas.*, vol. 69, no. 6, pp. 2924–2937, Jun. 2020.
[19] L. Yule, B. Zaghari, N. Harris, and M. Hill, "Surface temperature condition monitoring methods for aerospace turbomachinery: Exploring the use of ultrasonic guided waves," *Meas. Sci. Technol.*, vol. 32, no. 5, May 2021, Art. no. 052002.
[20] T. P. Jenkins, C. F. Hess, S. W. Allison, and J. I. Eldridge, "Measurements of turbine blade temperature in an operating aero engine using thermographic phosphors," *Meas. Sci. Technol.*, vol. 31, no. 4, Apr. 2020, Art. no. 044003.
[21] D. Li, C. Feng, S. Gao, K. Daniel, and L. Chen, "Effect of pyrometer type and wavelength selection on temperature measurement errors for turbine blades," *Infr. Phys. Technol.*, vol. 94, pp. 255–262, Nov. 2018.
[22] Z. Ji, F. L. Duan, and Z. Xie, "Transient measurement of temperature distribution using thin film thermocouple array on turbine blade surface," *IEEE Sensors J.*, vol. 21, no. 1, pp. 207–212, Jan. 2021.
[23] Q. Tan, W. Lv, Y. Ji, R. Song, F. Lu, H. Dong, W. Zhang, and J. Xiong, "A LC wireless passive temperature-pressure-humidity (TPH) sensor integrated on LTCC ceramic for harsh monitoring," *Sens. Actuators B, Chem.*, vol. 270, pp. 433–442, Oct. 2018.
[24] L. Lin, M. Ma, F. Zhang, F. Liu, Z. Liu, and Y. Li, "Integrated passive wireless pressure and temperature dual-parameter sensor based on LTCC technology," *Ceram. Int.*, vol. 44, pp. S129–S132, Nov. 2018.
[25] Y. Ji, Q. Tan, X. Lu, G. Zhang, W. Zhang, and J. Xiong, "Wireless passive separated LC temperature sensor based on high-temperature co-fired ceramic operating up to 1500 °C," *J. Micromech. Microeng.*, vol. 29, no. 3, Mar. 2019, Art. no. 035015.
[26] G. Zhang, Q. Tan, B. Lin, and J. Xiong, "A novel temperature and pressure measuring scheme based on LC sensor for ultra-high temperature environment," *IEEE Access*, vol. 7, pp. 162747–162755, 2019.
[27] Q.-A. Huang, L. Dong, and L.-F. Wang, "LC passive wireless sensors toward a wireless sensing platform: Status, prospects, and challenges," *J. Microelectromech. Syst.*, vol. 25, no. 5, pp. 822–841, Oct. 2016.
[28] C. Zhang, L.-F. Wang, J.-Q. Huang, and Q.-A. Huang, "An LC-type passive wireless humidity sensor system with portable telemetry unit," *J. Microelectromech. Syst.*, vol. 24, no. 3, pp. 575–581, Jun. 2015.
[29] Y. Ji, Q. Tan, H. Wang, W. Lv, H. Dong, and J. Xiong, "A novel surface LC wireless passive temperature sensor applied in ultra-high temperature measurement," *IEEE Sensors J.*, vol. 19, no. 1, pp. 102–112, Oct. 2019.

CHEN LI was born in 1987. He received the M.S. and Ph.D. degrees in intelligent instruments and measurement technology and instrument from the North University of China, Taiyuan, China, in 2014 and 2016, respectively. He is currently an Associate Professor with the Department of Instrumentation and Electronics, North University of China. His research interests include dynamic testing technology and micro-nano sensor devices in extreme environments.

MANGU JIA was born in Heihe, China, in 1997. She received the B.S. degree in measurement and control technology and instruments from the North University of China, Taiyuan, China, in 2019, where she is currently pursuing the M.S. degree in instrumentation engineering. Her research interest includes wireless passive rotational speed sensors.

YANAN XUE was born in Shuozhou, China, in 1995. She received the B.S. degree in measuring and testing technologies and instruments from the North University of China, Taiyuan, China, in 2018, where she is currently pursuing the M.S. degree in instrumentation engineering. Her research interest includes research on the preparation technology of wireless passive high-temperature vibration sensors.

YINGPING HONG was mainly engaged in pressure sensing method and integrated testing system under ultra-high temperature environment. His research interests include data recording and measuring equipment and instruments under super impact environment.

QIYUN FENG was born in Jingzhou, China, in 1997. She received the B.S. degree in measurement and control technology and instruments from Yanshan University, in 2020. She is currently pursuing the M.S. degree in instrumentation engineering from the North University of China. Her research interest includes fabrication of wireless passive sensors.

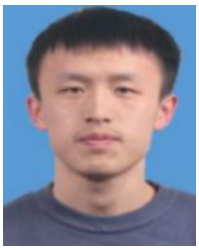

PENGYU JIA was born in Shuozhou, China, in 1995. He received the B.S. degree in mechanical design and manufacturing and automation from the North University of China, Taiyuan, China, in 2019, where he is currently pursuing the M.S. degree in instrumentation engineering. His research interest includes research on the preparation technology of the high-temperature pressure sensors.

HAOYUE LU was born in Zhengzhou, China, in 1999. She received the degree from the North University of China, Taiyuan, China, in 2018, where she is currently pursuing the degree in measurement and control technology and instrumentation. Her research interest includes fabrication of surface acoustic wave high temperature strain sensors.

JIJUN XIONG was born in 1971. He received the B.S. and M.S. degrees from the North University of China, Taiyuan, China, in 1993 and 1998, respectively, and the Ph.D. degree from Tsinghua University, Beijing, China, in 2003. He is currently a Professor and a Ph.D. Tutor. He is devoted to the fundamental theory and instrumentation research on dynamic mechanical parameters measurement for more than 20 years, mainly focused on the scale effect in silicon microstructures based the typical electromechanical conversion principle, the evolution law in the nanometer scale, and the applicable boundary scope under thermal environment.